Hearing Research 394 (2020) 107882

Contents lists available at ScienceDirect

Hearing Research

journal homepage: www.elsevier.com/locate/heares

Research Paper

Efficient viral transduction in mouse inner ear hair cells with utricle injection and AAV9-PHP.B

John Lee [a, 1], Carl Nist-Lund [a, 1], Paola Solanes [b], Hannah Goldberg [a], Jason Wu [a], Bifeng Pan [a], Bernard L. Schneider [b, c], Jeffrey R. Holt [a, *]

[a] Department of Otolaryngology & Neurology, Boston Children's Hospital and Harvard Medical School, Boston, MA, 02115, USA
[b] Brain Mind Institute, Ecole Polytechnique Fédérale de Lausanne, Station 19, 1015, Lausanne, Switzerland
[c] Bertarelli Platform for Gene Therapy, Ecole Polytechnique Fédérale de Lausanne, Station 19, 1015, Lausanne, Switzerland

ARTICLE INFO

Article history:
Received 8 November 2019
Received in revised form
27 December 2019
Accepted 1 January 2020
Available online 13 January 2020

ABSTRACT

Viral delivery of exogenous coding sequences into the inner ear has the potential for therapeutic benefit for patients suffering genetic or acquired hearing loss. To devise improved strategies for viral delivery, we investigated two injection techniques, round window membrane injection or a novel utricle injection method, for their ability to safely and efficiently transduce sensory hair cells and neurons of the mouse inner ear. In addition, we evaluated three synthetic AAV vectors (Anc80L65, AAV9-PHP.B, AAV2.7m8) encoding enhanced green fluorescent protein (eGFP) and three promoters (*Cmv, Synapsin, Gfap*) for their ability to transduce and drive expression in desired cell types. We found the utricle injection method with AAV9-PHP.B and a *Cmv* promoter was the most efficient combination for driving robust eGFP expression in both inner and outer hair cells. We found eGFP expression levels rose over 3–5 days post-injection, a viral dose of 1.5×10^9 gc yielded half maximal eGFP expression and that the utricle injection method yielded transduced hair cells even when delivered as late as postnatal day 16. Sensory transduction and auditory thresholds were unaltered in injected mice relative to uninjected wild-type controls. Vestibular end organs were also transduced without affecting balance behavior. The *Synapsin* promoter and the *Gfap* promoter drove strong eGFP expression in inner ear neurons and supporting cells, respectively. We conclude the AAV9-PHP.B vector and the utricle injection method are well-suited for delivery of exogenous gene constructs into inner ears of mouse models of auditory and vestibular dysfunction.

1. Introduction

Inner ear gene therapy, the delivery of therapeutic DNA constructs for restoration of hearing and balance function or prevention of inner ear dysfunction, is a nascent field. However, in recent years a number of paradigm-shifting studies have presented tantalizing proof-of-concept data demonstrating that viral delivery of gene therapy reagents into the inner ear can prevent hearing loss or recover function in mouse models of genetic deafness (Akil et al., 2012; Askew et al., 2015; Chien et al., 2016; Emptoz et al., 2017; György et al., 2017, 2019; Pan et al., 2017; Dulon et al., 2018; Nist-Lund et al., 2019). While encouraging, the success of these approaches has been limited by the lack of viral capsids that efficiently transduce the desired target cells. Conventional AAV vectors, while useful for targeting other cell types, do not efficiently transduce sensory hair cells (Kilpatrick et al., 2011; Askew et al., 2015; Tao et al., 2018; Gu et al., 2019). Several synthetic AAV capsids have been developed and reported to offer higher hair cell transduction efficiencies (Landegger et al., 2017; Suzuki et al., 2017; Isgrig et al., 2019; György et al., 2019), but results vary and higher efficiency vectors with more thorough characterization are needed.

Here we focus on a comparative analysis between two different injection methods and several synthetic vector capsids including AAV2.7m8 (Dalkara et al., 2013), Anc80L65 (Zinn et al., 2015) and AAV9-PHP.B (Deverman et al., 2016). We find enhanced transduction efficiencies with a novel injection method developed to deliver gene therapy vectors into endolymphatic spaces with minimal toxicity. We also find that direct injection into the utricle is equal to or superior to round window membrane (RWM) injection,

* Corresponding author.
E-mail address: jeffrey.holt@childrens.harvard.edu (J.R. Holt).
[1] Equal contribution.

https://doi.org/10.1016/j.heares.2020.107882

and drives efficient viral transduction and eGFP expression in hair cells and neurons.

We report that of the three synthetic AAV capsids investigated, AAV9-PHP.B had the highest efficiency transduction in both inner and outer hair cells and robust transduction in spiral and vestibular ganglion neurons. We conclude that AAV9-PHP.B may be well-suited for further development and perhaps translation to human clinical application for the treatment of genetic inner ear disorders.

2. Results

2.1. Utricle injection method

To identify vectors and delivery methods that provide efficient viral transduction in inner and outer hair cells and spiral ganglion neurons, we compared two delivery methods and three synthetic adeno-associated viral vectors. Intracochlear injection through the round window membrane (RWM) has been demonstrated as a safe and feasible method for delivery of viral vectors into the perilymphatic space of the inner ear (Akil et al., 2012; Askew et al., 2015). However, there are several shortcomings of this delivery method including limited viral transduction from base to apex, limited transduction of outer hair cells and inability to access endolymphatic spaces. Cochleostomy allows direct access to endolymph and improved viral transduction of outer hair cells, but carries additional risk of cochlear damage due to rupture of the endolympatic − perilympatic barrier which separates high K+ endolymph from perilymph. To circumvent these limitations we explored an alternate delivery route into the inner ear. We developed an injection method into the utricle, one of two otolith organs sensitive to linear acceleration and gravity. We reasoned that the sac-like anatomical structure of the utricle would allow easier access to the endolymphatic compartment, while minimizing risk of disrupting the cochlear partition. Since endolymphatic solutions are confluent throughout the cochlea and vestibular organs, we anticipated broad viral distribution. The site of utricle injection is illustrated in Fig. 1A. To evaluate the utricle injection approach relative to RWM injection, we delivered 1 μL of Anc80L65-*Cmv*-eGFP at postnatal day one (P1). Cochlear tissue was harvested four weeks post-injection, fixed and stained with anti-Myo7A to label hair cells. Samples were imaged by confocal microscopy using identical acquisition and analysis parameters. Low-magnification images revealed eGFP fluorescence throughout the cochlea with both injection methods (Fig. 1B and C). Higher magnification (63x) images were taken from the apical (8 kHz), middle (16 kHz) and basal (32 kHz) regions of the cochlea (Fig. 1D) and revealed eGFP expression in both inner and outer hair cells. Non-hair cells were also eGFP-positive, including pillar cells and Deiter's cells. Since eGFP fluorescence varies among cells, we quantified eGFP-positive hair cells as a percentage of total Myo7a-positive hair cells, scored by three blinded investigators. We took the mean value for the three investigators and plotted the data from six mice, three for each injection method (Fig. 1E). For the RWM-injected mice, 90–100% of IHC and 40–90% of OHC were transduced, consistent with prior quantification (Landegger et al., 2017). In cochleas of utricle-injected mice, 100% of IHCS in all three regions were GFP-positive and 30–90% of OHCs were GFP-positive depending on the region. In general, we found a higher percentage of GFP-positive OHCs in the apex than in the base for both injection methods. The utricle injection method yielded slightly higher transduction rates in IHCs and OHCs than RWM injection. Overall, across all three samples and the three regions of the cochlea, we found 71% of hair cells were eGFP-positive following RWM injection. With utricle injection we found 76% of the hair cells were eGFP-positive. We did not observe GFP fluorescence in the contralateral inner ear following utricle injection, in contrast to that reported previously for RWM injection (Landegger et al., 2017).

2.2. AAV9-PHP.B capsids efficiently transduce hair cells

Recent reports suggest that AAV9-PHP.B, an AAV variant that broadly and efficiently transduces cells of the central nervous system (Deverman et al., 2016), also targets IHCs and OHCs when injected via the RWM (György et al., 2019; Kim et al., 2019). To evaluate transduction efficiency of the AAV9-PHP.B capsid relative to that of the Anc80L65 capsid, we examined both RWM and utricle injection methods using 1 μL AAV9-PHP.B-*Cmv*-eGFP. Fig. 2A − C show low magnification confocal images of the apical and basal halves of cochleas injected at P1 via the RWM or utricle as described above. High viral transduction efficiency for both IHCs and OHCs was evident with significantly less eGFP fluorescence in other cell types. High magnification images of 100-μm sections revealed strong eGFP fluorescence in nearly all IHCs and OHCs in the apical (8 kHz), mid (16 kHz) and basal (32 kHz) regions of the cochlea (Fig. 2D). Three blinded investigators independently quantified the number of eGFP-positive hair cell as a percentage of Myo7a-positive hair cells in 100-μm cochlear sections from three mice injected using the two methods (Fig. 2E). The data reveal that the AAV9-PHP.B capsid had higher hair cell transduction efficiency and specificity relative to the Anc80L65 capsid. Furthermore, the utricle injection method targeted nearly 100% of IHCs and OHCs in all regions of the cochlea, whereas the RWM approach was more variable with one cochlea showing 40–70% OHC transduction. Overall, RWM injection of AAV9-PHP.B yielded 88% hair cell transduction and utricle injection yielded 99% eGFP-positive hair cells.

2.3. Three synthetic AAV capsids target hair cells

Because viral production protocols and titers can vary with production facility, we opted to confirm our results by comparing equivalent titer injections of AAV9-PHP.B-*Cmv*-eGFP or Anc80L65-*Cmv*-eGFP produced by a single facility, the Vector Core at Boston Children's Hospital. We also evaluated a third vector, AAV2.7m8-*Cmv*-eGFP, another synthetic capsid recently reported to transduce mouse inner ear hair cells (Isgrig et al., 2019), at the equivalent titer and produced in the same facility. Ten P1 C57BL/6 mouse pups were injected via the utricle with 1 μL containing 3.5×10^9 gc of one of the three vectors. Two weeks post-injection, cochleas were harvested and imaged for eGFP fluorescence (Fig. 3A–C). The mean percentages of eGFP-positive IHCs and OHCs were scored by three investigators blinded to the viral capsid. The images and data revealed that AAV9-PHP.B-*Cmv*-eGFP displayed the highest transduction efficiency with 80–100% of hair cells transduced in all tonotopic regions of the cochlea. Anc80L65 and AAV2.7m8 had lower efficiencies and more variable transduction in both IHCs and OHCs in all regions of the cochlea.

2.4. AAV9-PHP.B injection at later stages drives gene expression

To investigate exogenous gene expression at later stages, six mice were injected via the utricle at P7 or P16 with either AAV9-PHP.B-*Cmv*-eGFP or Anc80L65-*Cmv*-eGFP (Fig. 4). The percentage of eGFP-positive hair cells was quantified as described previously. We found that AAV9-PHP.B drove eGFP expression in 100% of IHCs in all three mice at both P7 and P16 (Fig. 4A and B). Eighty to 100% of OHCs were also GFP-positive at P7.

While the efficiency of eGFP expression in OHCs was lower at P16 than at P7 with AAV9-PHP.B, transduction efficiency in both IHCs and OHCs was higher than for mice injected with Anc80L65 at

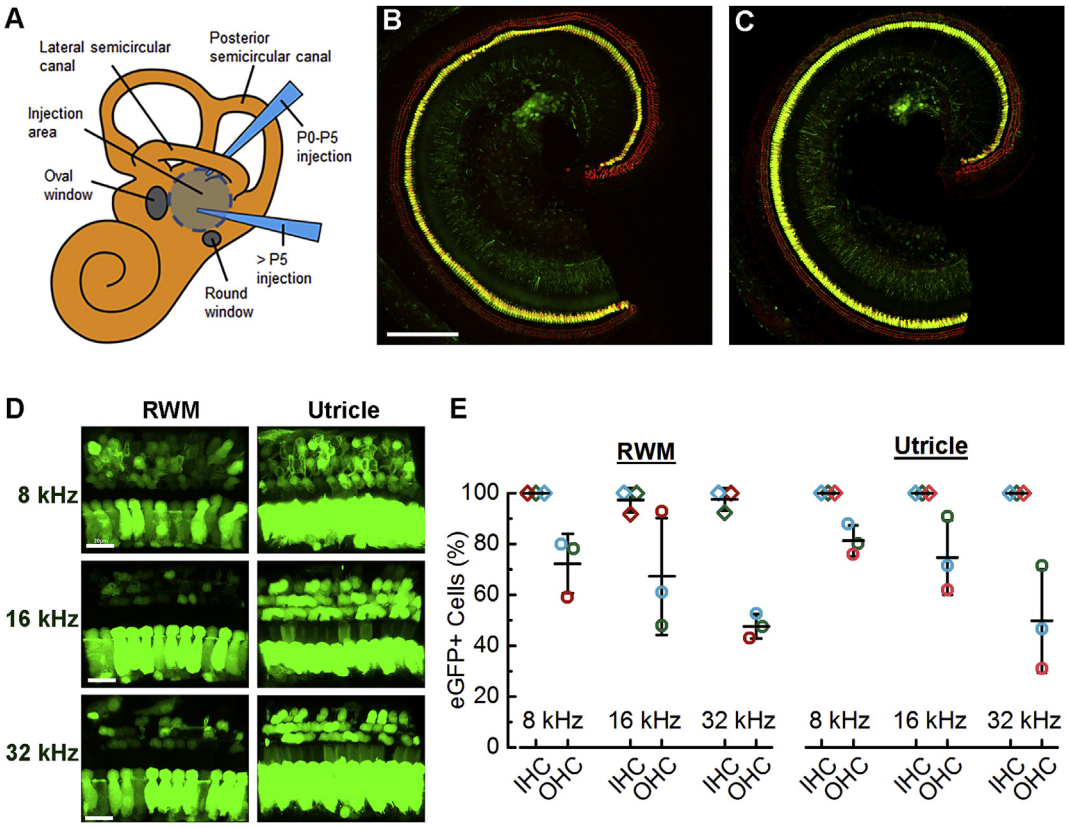

Fig. 1. Utricle injection method vs RWM with Anc80L65-*Cmv*-eGFP. (**A**) A schematic diagram of cochlea illustrating the two utricle injection sites used in this study. (**B**) Representative confocal image from the apex of a cochlea injected with 1 μL of Anc80L65-*Cmv*-eGFP at P1 via RWM (**B**) or utricle (**C**). Temporal bones were harvested at 4 weeks. Hair cells were stained with anti-Myosin 7a (red) with eGFP shown in green. Scale bars = 100 μm. (**D**) High magnification confocal images (63x) of eGFP fluorescence from apical, middle and basal regions of cochleas injected with 1 μL of Anc80L65-*Cmv*-eGFP at P1 via RWM or utricle as indicated. Scale bars = 20 μm. (**E**) Percentage of eGFP-positive IHCs and OHCs quantified in 100-μm sections by three investigators blinded to the conditions. Counts were taken from images as shown in panel D from three mice for each injection method. Symbol colors represent different mice. Mean ± S.D. are indicated for IHCs and OHCs for each of three frequency regions. (For interpretation of the references to color in this figure legend, the reader is referred to the Web version of this article.)

P7 and P16. (Fig. 4C and D). Later time points were not tested.

2.5. Exogenous gene expression as a function of time and titer

To evaluate exogenous gene expression as a function of time post-injection, we injected 15 wild-type P1 mice via the utricle with 1 μL of AAV9-PHP.B-*Cmv*-eGFP and harvested cochleas at 24-h intervals between one and five days post-injection. The tissue was stained with anti-Myo7a and an Alexfluor633 secondary antibody. Faint eGFP fluorescence was evident as early as one day post-injection (Fig. 5A). Fluorescence intensity rose steadily over the subsequent few days. Nearly 100% of IHCs and OHCs were strongly fluorescent by four and five days post-injection. (Fig. 5A). To quantify the rise in eGFP fluorescence as a function of time we used identical image acquisition and analysis parameters and calculated the mean fluorescence intensity for each eGFP image. Representative images were acquired from basal, middle and apical regions of the cochlea. Mean fluorescence intensity, in arbitrary units, was plotted as function of time post-injection and demonstrated a steady rise in exogenous gene expression within a few days post-injection (Fig. 5B).

To evaluate eGFP fluorescence as a function of titer, we injected eight wild-type mice at P1 with 1 μL of AAV9-PHP.B-*Cmv*-eGFP in doses that ranged between 3.5×10^8 and 3.5×10^9 gc. Cochleas were harvested at P14 and imaged for eGFP fluorescence. Fig. 5C shows four representative images from the 100-μm apical sections acquired and analyzed with identical image parameters. Both the number of eGFP-positive hair cells and the fluorescence intensity increased as a function of increasing titer. We quantified the relative change in eGFP fluorescence intensity across each entire image and plotted the data as a function of viral dose (Fig. 5D). The data were fitted with a Boltzmann equation which reveal a steep relationship and a half maximal dose of 1.5×10^9 gc.

2.6. AAV9-PHP.B transduction does not alter auditory function

To determine whether utricle injection or viral transduction with AAV9-PHP.B-*Cmv*-eGFP disrupts auditory function, we recorded sensory transduction currents from eGFP-positive IHCs and OHCs following P1 injection. Cochleas were excised at P5-7 and incubated in MEM with 1% FBS for up to 3 weeks at 37 °C, 5% CO_2. Sensory transduction currents were recorded by deflecting hair bundles from −200–1050 nm with a stiff glass probe mounted on a piezo-electric bimorph (Stauffer and Holt, 2007). Hair cells were voltage-clamped at −84 mV and transduction currents were recorded from eGFP-positive cells and eGFP-negative control cells between P7 and P29. Fig. 6A shows representative families of transduction currents recorded from an eGFP-positive P7 OHC and eGFP-positive P7 and P29 IHCs, revealing current amplitudes and adaptation similar to eGFP-negative wild-type cells. For the OHC currents, mean transduction currents of ~1200 pA were measured, while at later time points the currents declined to ~800 pA at P13 and ~600 pA at P16 (Fig. 6B). For IHCs mean currents of ~900 pA were measured at P7, with mean currents of ~600 pA between at

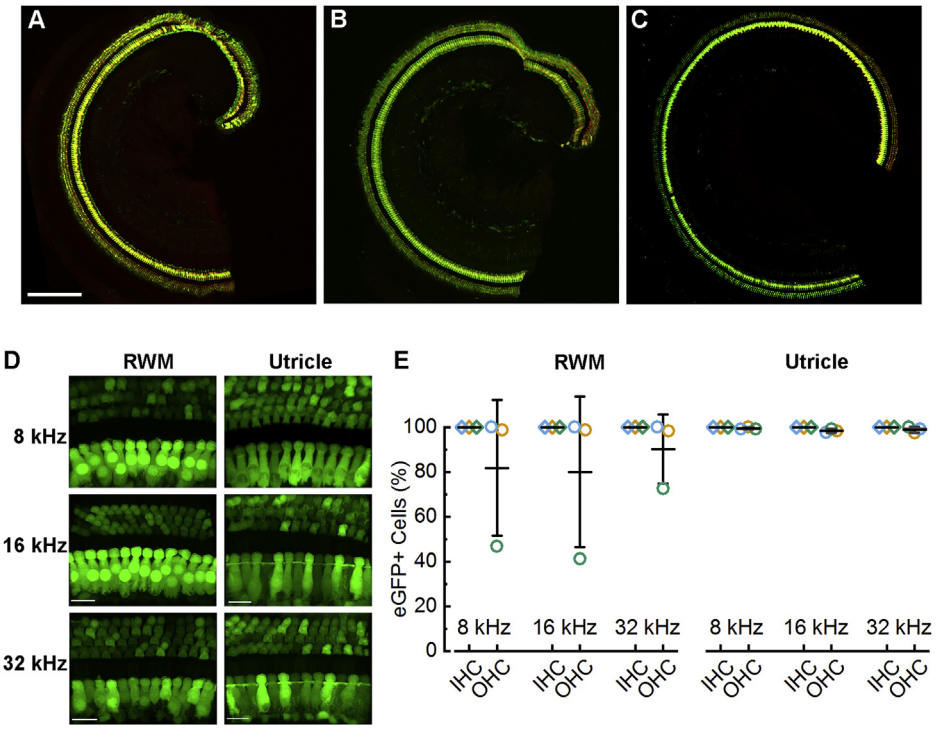

Fig. 2. Utricle injection method vs RWM with AAV9-PHP.B-Cmv-eGFP. Representative confocal images from apical cochlear sections of mice injected with 1 μL of AAV9-PHP.B-*Cmv*-eGFP via the RWM (**A**) or utricle (**B**) or basal region from a utricle-injected inner ear (**C**). Scale bars = 100 μm and applies to panels A–C. Temporal bones were harvested at 4 weeks. Hair cells were stained with anti-Myosin 7a (red) with eGFP shown in green. (**D**) High magnification confocal images (63x) of eGFP fluorescence from apical, middle and basal regions of cochleas injected with 1 μL of AAV9-PHP.B-*Cmv*-eGFP at P1 via RWM or utricle as indicated. Scale bars = 20 μm. (**E**) Percentage of eGFP-positive IHCs and OHCs quantified in 100-μm sections by three investigators blinded to the conditions. Counts were taken from images as shown in panel D from three mice for each injection method. Symbol colors represent different mice. Mean ± S.D. are indicated for IHCs and OHCs for each of three frequency regions. (For interpretation of the references to color in this figure legend, the reader is referred to the Web version of this article.)

P13 and P29. Transduction amplitudes currents from AAV9-PHP.B-*Cmv*-eGFP transduced hair cells were similar to those previously reported for Anc80L65-*Cmv*-eGFP transduced hair cells and eGFP-negative control cells (Landegger et al., 2017). To investigate hair bundle sensitivity, we generated current-displacement (I-X) curves from eGFP-positive OHCs, which were fitted with 2nd order Boltzmann equations that had 10–90% operating ranges similar to those of eGFP-negative wild-type cells hair cells (Fig. 6C).

Next, we recorded Auditory Brainstem Responses (ABRs) and Distortion Product Otoacoustic Emissions (DPOAEs) from 36 mice that received utricle injections of AAV9-PHP.B-*Cmv*-eGFP or Anc80L65-*Cmv*-eGFP to determine if there were any detrimental effects on cochlear function. Only mice with confirmed cochlear expression of eGFP were included in the ABR/DPOAE analysis. Mice were injected at P1, P7 or P16 via the utricle and measurements were made at one month of age. We found no significant differences in ABR or DPOAE threshold for any frequency, age of injection or vector capsid, relative to uninjected wild-type mice (Fig. 6D–F). In summary, the single cell electrophysiology data and ABR/DPOAE data indicate that the utricle injection method and AAV9-PHP.B-*Cmv*-eGFP vectors do not cause auditory dysfunction.

2.7. Synthetic AAV vectors drive exogenous gene expression in vestibular organs

Although genetic vestibular dysfunction has been poorly characterized, viral delivery of exogenous genetic material into vestibular organs may provide a future therapeutic avenue. As such, we imaged eGFP fluorescence in vestibular end organs of mice injected via the utricle at P1, P7 and P16. We found AAV9-PHP.B-*Cmv*-eGFP drove robust eGFP expression in the utricle, saccule and crista ampullaris of all three semicircular canals at all time points tested (Fig. 7). In contrast, eGFP expression was qualitatively lower with later stage injections of Anc80L65-*Cmv*-eGFP, particularly in the utricle and cristas (Fig. 7A). Robust hair cell transduction was also observed in saccules of AAV9-PHP.B-*Cmv*-eGFP injected mice at all three time points (Fig. 7B).

To quantify eGFP expression in vestibular organs as a function of time, we injected 15 wild-type P1 mice via the utricle with 1 μL of AAV9-PHP.B-*Cmv*-eGFP and harvested cochleas at 24-h intervals between one and five days post-injection. We measured the change in eGFP expression using identical image acquisition and analysis parameters and calculated the mean eGFP fluorescence intensity per unit area for the entire sensory epithelium for utricles and saccules. Faint eGFP fluorescence was evident as early as one day post-injection. Within three days post-injection, fluorescence intensity reached a stable plateau (Fig. 7C).

To evaluate eGFP fluorescence in vestibular organs as a function of viral dose we injected eight wild-type mice at P1 with 1 μL of AAV9-PHP.B-*Cmv*-eGFP and doses that ranged between 3.5×10^8 and 3.5×10^9 gc. Utricles and saccules were harvested at P14 and imaged for eGFP fluorescence as described above. eGFP fluorescence intensity increased as a function of viral dose (Fig. 7D). The data were fitted with a Boltzmann equation which reveal a steep relationship and a half maximal dose of 6.7×10^8 gc.

We observed no adverse behaviors typically associated with vestibular dysfunction, such as circling or head bobbing, in utricle injected mice. To further evaluate safety and possible deleterious effects of utricle injection and AAV9-PHP.B-*Cmv*-eGFP transduction, we measured balance behavior at six weeks of age in utricle-

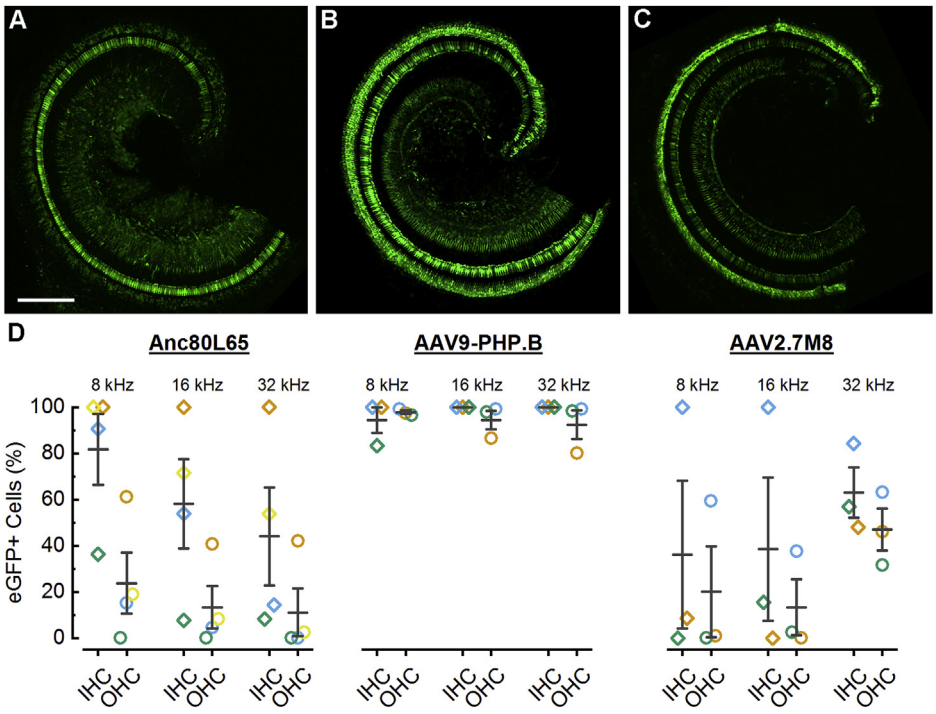

Fig. 3. Comparison of three synthetic AAVs at equivalent titers. (A) Representative confocal images of the apical region of cochleas from mice injected via the utricle at P1 with 1 μL (3.5×10^9 gc) of one of the three vectors: (**A**) Anc80L65-*Cmv*-eGFP, (**B**) AAV9-PHP.B-*Cmv*-eGFP or (**C**) AAV2.7m8-*Cmv*-eGFP. Temporal bones were harvested at 2 weeks and cochleas were mounted and imaged for eGFP fluorescence. Scale bars = 100 μm and applies to panels A–C. (**D**) Percentage of eGFP-positive IHCs and OHCs quantified from high magnification (63x) images by three investigators blinded to the conditions. Counts were taken from in 100-μm sections similar to those shown in Fig. 2D from three - four mice for each vector. Symbol colors represent different mice. Mean ± S.D. are indicated for IHCs and OHCs for each of three frequency regions. (For interpretation of the references to color in this figure legend, the reader is referred to the Web version of this article.)

injected mice using a rotarod assay. While the rotarod assesses both balance and motor function, mice with poor vestibular function typically perform poorly on the assay. Uninjected wild-type mice balanced on the rod for 120 ± 8.7 s (mean ± S.D., $n = 5$ trials) which was not significantly different ($p = 0.56$) from utricle-injected mice which remained balanced on the rod for 112 ± 8.7 s (n = 3 mice). We also tested vestibular evoked potentials (VsEPs; Jones et al., 2002) in six mice and found no significant difference ($p = 0.51$) between VsEP thresholds in utricle-injected mice (−4.5 ± 2.1 dB) and uninjected controls (−6 ± 2.4 dB). Postmortem histological analysis confirmed eGFP expression in vestibular organs of rotarod- and VsEP-tested mice. We conclude that utricle injection and viral transduction with AAV9-PHP.B-*Cmv*-eGFP do not adversely affect vestibular function as determined by these assays.

2.8. AAV9-PHP.B transduction in other cell types

To investigate AAV9-PHP.B-*Cmv*-eGFP transduction and expression in other cell types, we generated cochlear cryo-sections from mice that received utricle injections at P1. Tissue sections were counter-stained with anti-Myo7a and an Alexfluor633 secondary antibody, anti-Tuj1, a neuronal cell marker, and an Alexa Fluor 547 secondary and DAPI. eGFP-positive cells were apparent in the organ of Corti, primarily in hair cells, and in the spiral limbus and spiral ligament (Fig. 8A). Sporadic eGFP fluorescence was evident throughout the lateral walls of the cochlea but there was little fluorescence in neurons of the spiral ganglia. In the vestibular end organs, eGFP fluorescence was restricted to hair cells of the utricle, saccule and crista ampullaris (Fig. 8B).

Since AAV9-PHP.B was previously reported to transduce spiral ganglion neurons (Keppeler et al., 2018), we investigate whether the capsid was capable of transducing and driving exogenous gene expression in neurons of the spiral and vestibular ganglia using a *Synapsin* (*Syn*) promoter to drive eGFP expression: AAV9-PHP.B-*Syn*-eGFP. In the inner ear, the *Syn* promoter drives expression in SGNs (Hernandez et al., 2014; Askew et al., 2015; Keppeler et al., 2018). The AAV9-PHP.B-*Syn*-eGFP construct (1 μL) was injected via the utricle at P1 and cryo-sections were generated and stained as described above. Consistent with the prior reports, we observed robust eGFP fluorescence in spiral ganglion neurons, but no other cell type in the cochlea (Fig. 8C). Likewise, in the vestibular organs, there was prominent eGFP fluorescence in the vestibular ganglion neuron cell-bodies, fiber tracks and in synaptic terminals in vestibular end organs, but no other cell type (Fig. 8D). The data suggest that the AAV9-PHP.B capsid is capable transducing both hair cells and neurons and that the *Syn* promoter can be used selectively in the inner ear to drive expression in neurons.

Lastly, we investigated whether an alternate promoter might be useful for driving expression in supporting cells. We generated vectors with a *Gfap* promoter driving eGFP expression. The construct was packaged as AAV9-PHP.B-*Gfap*-eGFP and 1 μL was injected into the utricle at P1. In the cochlea we observed eGFP fluorescence in supporting cells of the spiral limbus and in pillar cells in the Organ of Corti, but not in hair cells (Fig. 9A). In the utricle we found robust eGFP expression in supporting cells throughout the epithelium but not in hair cells (Fig. 9B and C). The data support use of AAV9-PHP.B capsid and the *Gfap* promoter for driving exogenous gene expression in supporting cells of the cochlea and vestibular organs.

3. Discussion

Here we developed and characterized a novel injection method for safe and efficient delivery of viral vectors into all six sensory

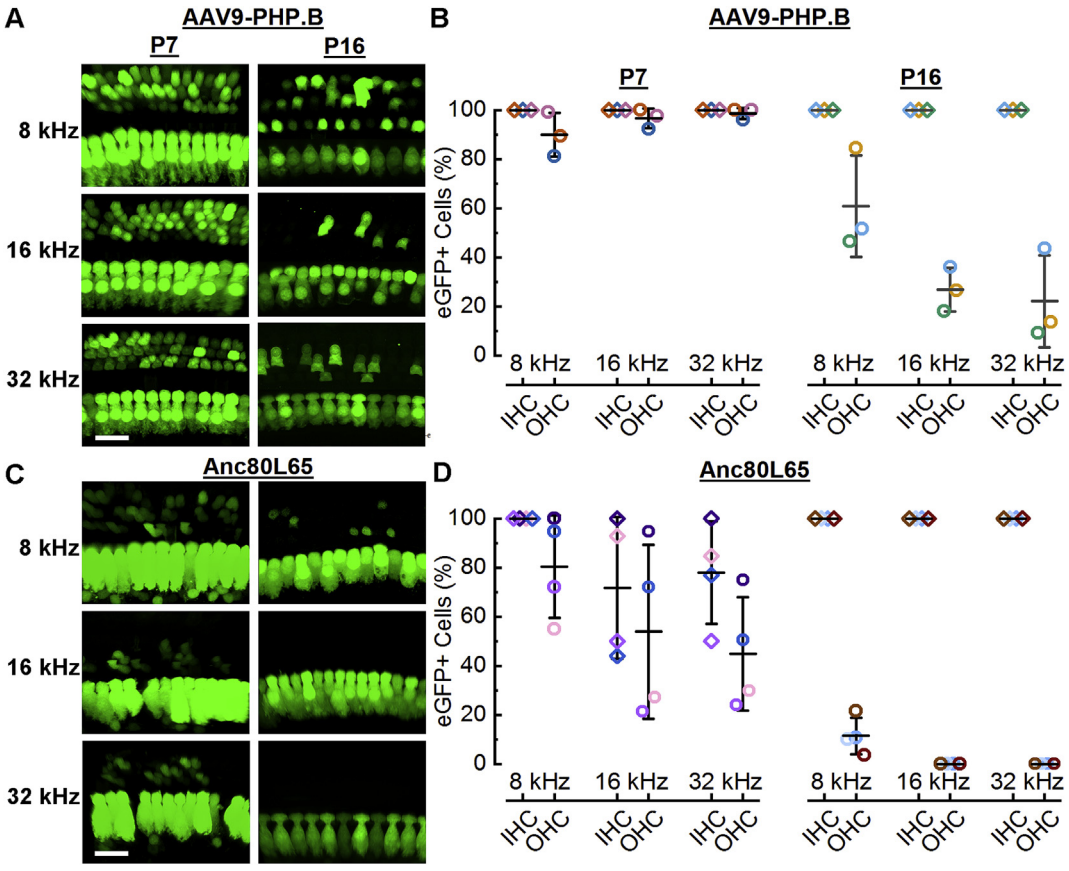

Fig. 4. Viral transduction following utricle injections at P7 and P16. (**A**) Representative 100-μm confocal images (63x) of eGFP fluorescence in apical, middle and basal regions of cochleas injected with 1 μL of AAV9-PHP.B-*Cmv*-eGFP at P7 or P16 via the utricle as indicated. Scale bar = 20 μm. (**B**) Percentage of eGFP-positive IHCs and OHCs from cochleas injected with 1 μL of AAV9-PHP.B-*Cmv*-eGFP at P7 or P16 via the utricle as indicated. Cell counts were quantified by three investigators blinded to the conditions. Counts were taken from in 100-μm sections as shown in panel A from three mice at each injection stage. Symbol colors represent different mice. Mean ± S.D. are indicated for IHCs and OHCs for each of three frequency regions. (**C**) 100-μm confocal images of eGFP fluorescence in apical, middle and basal regions of cochleas injected with 1 μL of Anc80L65-*Cmv*-eGFP at P7 or P16 via the utricle as indicated. Scale bar = 20 μm. (**D**) Percentage of eGFP-positive IHCs and OHCs from cochleas injected with 1 μL of Anc80L65-*Cmv*-eGFP at P7 or P16 via the utricle as indicated. Cell counts were quantified by three investigators blinded to the conditions. Counts were taken from in 100-μm sections as shown in panel C from three mice at each injection stage. Symbol colors represent different mice. Mean ± S.D. are indicated for IHCs and OHCs for each of three frequency regions. (For interpretation of the references to color in this figure legend, the reader is referred to the Web version of this article.)

organs of the inner ear. We found the utricle injection technique to be reliable, reproducible and a technically approachable skill that novice injectors were able to acquire more rapidly. While our goal was to target the endolymphatic compartments of the inner ear, we did not have an independent assay to confirm whether the injected vectors were restricted to that fluid compartment or whether some gained access to perilymphatic compartments. Given that in some experiments we observed eGFP fluorescence in spiral and vestibular ganglion neurons, we suspect the AAV9-PHP.B must have accessed the perilymphatic space. Indeed, the AAV9-PHP.B capsid was originally generated and selected for its ability to cross the blood-brain barrier (Deverman et al., 2016). Whether this ability extends to the blood-labrynthine barrier or endolymph-perilymph barrier remains a possibility. However, given the small volume and dose of viral vector injected into the inner ear, ~1 × 10^9 gc suspended in 1 μL, the concern for off-target effects outside of the ear remains minimal. While the utricle injection approach may not be as easily accessible for clinical application as the RWM approach, which is routinely used for cochlear implants, the utricle approach offers the advantage of direct delivery to endolymphatic fluids with no apparent loss of hearing or balance function. We conclude the strategy represents a viable alternative to cochleostomy or RWM injection and may help advance pre-clinical studies in mouse models of genetic and acquired hearing loss.

We also find that the AAV9-PHP.B capsid provides higher efficiency transduction in inner and outer hair cells than two other synthetic vectors, Anc80L65 (Landegger et al., 2017) and AAV2.7m8 (Isgrig et al., 2019). The biological basis of this difference is not clear but may be the result of the seven additional amino acids, TLAVPFK, within the protein coat of the AAV9-PHP.B capsid. The TLAVPFK sequence emerged through a directed evolution approach and was selected based on the ability to cross the blood-brain barrier when injected intravenously into the peripheral circulation (Deverman et al., 2016). This same property may provide an advantage for viral transduction within the cochlea.

Our results with AAV9-PHP.B are consistent with and extend the observations of two other groups who recently evaluated the AAV9-PHP.B capsid (György et al., 2019; Kim et al., 2019). Although the two other groups reported high transduction efficiencies in inner hair cells, their reported efficiencies in outer hair cells were lower than those we report here. Kim et al. (2019) had OHC transduction efficiencies of 20–60% and György et al. (2019) reported efficiencies of 30–70%, both significantly less than our mean values of 90–100%. However, we do note several differences between the three studies that may account for the apparent discrepancy. Both prior studies used RWM injection and titers that were lower than those presented here. In addition, György et al. (2019) used a different promoter, CBA, while Kim et al. and we used a CMV

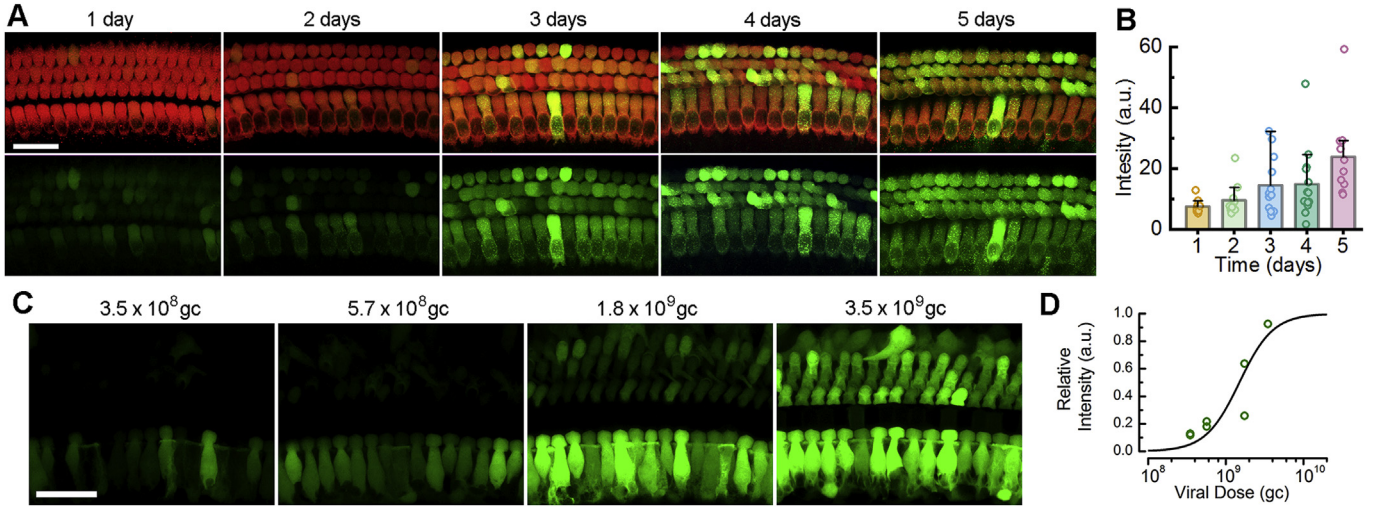

Fig. 5. Exogenous gene expression as function of time. (**A**) Representative confocal images of 100-μm apical cochlear sections from mice injected with 1 μL of AAV9-PHP.B-*Cmv*-eGFP at P1 via the utricle. The tissue was harvested between one and five days post-injection, fixed, stained with anti-Myo7a and mounted for imaged for eGFP fluorescence (green) and Myo7a (red) using identical image acquisition and analysis parameters. Upper panels show the two channels merged. Lower panels show eGFP fluorescence alone. Scale bar = 20 μm. (**B**) Mean eGFP fluorescence intensity was measured for each cochlear section taken from apical, middle and basal sections of three mice injected with 1 μL of AAV9-PHP.B-*Cmv*-eGFP at P1 via the utricle. Symbols represent fluorescence intensity in arbitrary units (a.u.) for each image plotted as a function of age. Bars represent the mean value +S.D. for each time point. (**C**) Confocal images of 100-μm cochlear sections from the apex of mice injected with 1 μL of AAV9-PHP.B-*Cmv*-eGFP at P1 via the utricle. The viral stock was diluted in PBS to the viral dose indicated above each panel. Cochleas were harvested at P14. Cochleas were fixed, stained with anti-Myo7a, mounted and imaged for eGFP fluorescence (green) using identical image acquisition and analysis parameters. Scale bar = 25 μm. (**D**) Mean eGFP fluorescence intensity was measured for each cochlear section taken from the apical region of two mice for each dose. Symbols represent the relative intensity in arbitrary units (a.u.). The values were fit with a first order Boltzmann equation (line) that had a midpoint of 1.5×10^9 gc. (For interpretation of the references to color in this figure legend, the reader is referred to the Web version of this article.)

promoter. Of the several differences in study design, we suspect the injection technique itself, RWM vs utricle, may have been the most salient difference, leading to higher OHC transduction efficiency in the present study.

Lastly, we report here that alternate promoters, *Syn* and *Gfap,* can be used in combination with AAV9-PHP.B capsids to drive selective expression in subsets of cochlear cell types, such as neurons and supporting cells. We conclude that the AAV9-PHP.B capsid is a powerful vector for driving exogenous gene expression in preclinical mouse models of hearing and balance disorders and may be well-suited for further development and perhaps translation to clinical application as a gene therapy vehicle for treatment of inner ear dysfunction in humans.

4. Materials and methods

4.1. Viral vector preparations

All viral vectors used for this study were generated and produced by the Viral Core at Boston Children's Hospital (BCH) and were used under the authority of the BCH Institutional Biosafety Committee (protocol # IBC-P00000447). AAV vectors were purified by iodixanol gradient ultracentrifuge, followed by ion exchange chromatography. Titers were calculated by quantitative PCR with GFP primers (F-GACCTTTGGTCGCCCGGCCT, R-GAGTTGGCCACTCCCTCTCTGC). The titer of Anc80-*Cmv*-eGFP-WPRE was 1.4×10^{13} gc/mL, AAV9-PHP.B-*Cmv*-eGFP-WPRE 3.5×10^{12} gc/mL and for AAV2.7m8-*Cmv*-eGFP-WPRE was 6.2×10^{12} gc/mL. AAV9-PHP.B-*Syn*-eGFP-WPRE 2.4×10^{12} gc/mL and AAV9-PHP.B-*Gfap*-eGFP was 3.7×10^{13} gc/mL. Vectors were aliquoted, stored at −80 °C and thawed immediately prior to use.

4.2. Inner ear injections

Utricle and round window membrane (RWM) injections were performed as approved by the Institutional Animal Care and Use Committees at Boston Children's Hospital (protocol #18-01-3610R and #17-03-3396R). The utricle and RWM were identified visually with the aid of a steromicroscope (Zeiss Stemi 2000). One microliter of vector was injected in neonatal wild-type mice (C57BL6) at P1, P7 or P16. Mice (P1 and P7) were anesthetized using hypothermia exposure on ice, while older mice (P16) were anesthetized with isoflurane. Upon anesthesia, post-auricular incision was made to expose the otic bulla and visualize the semicircular canals. Injections were done through the utricle with a glass micropipette filled with AAV vectors or through the RWM as previously described (Askew et al., 2015). Standard post-operative care was applied after the injection.

4.3. Tissue preparation and immunostaining

Temporal bones were harvested from mice euthanized with CO_2 and fixed for 1 h at room temperature with 4% paraformaldehyde in PBS, followed by decalcification with 120 mM ethylene diamine tetraacetic acid (EDTA), pH = 7.4 (6 h for 2 weeks old or 24 h for 4 weeks old). Cochlear sections were isolated (apex, mid and base) and tectorial membranes and lateral walls were removed under a dissection microscope. Vestibular epithelia (utricle, saccule, three semicircular canal cristae) were also isolated and the pigmented roof epithelium of each end organ was removed. For immunostaining, cochlear tissues were permeabilized with 0.1% Triton-X in PBS for 1 h at room temperature and blocked in 2.5% normal donkey serum and 2.5% bovine serum albumin diluted in PBS (blocking solution) for 1 h at room temperature. Tissues were then incubated with a rabbit anti-Myosin 7a antibody (Proteus Biosciences, 1:500 dilution in blocking solution) as a hair cell marker at 4 °C overnight. A donkey anti-rabbit antibody conjugated to Alexa Fluor 633 (Life Technologies, 1:200) was used as the secondary antibody to visualize inner and outer hair cells. Vestibular tissues were permeabilized with 0.3% Triton-X in PBS for 45 min at room temperature and blocked in 5% normal horse serum

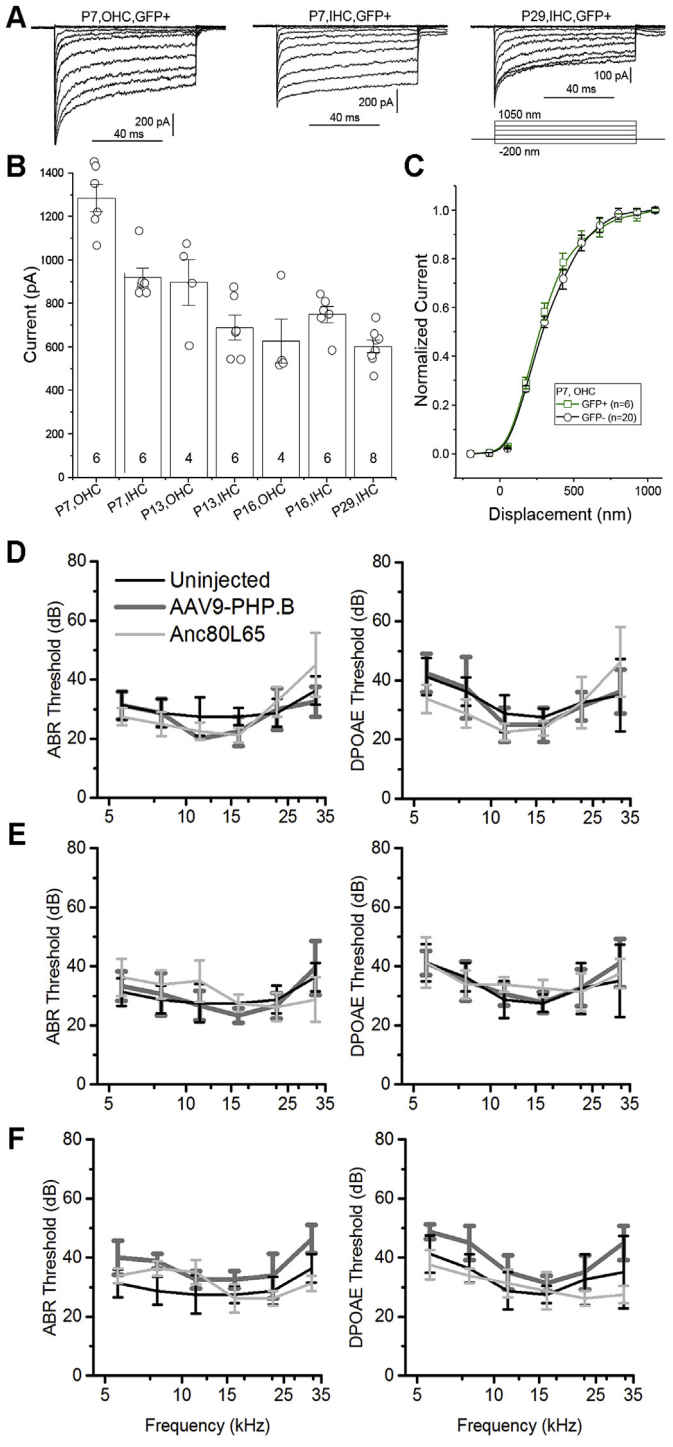

Fig. 6. Sensory transduction currents, ABRs and DPOAEs from injected mice. (**A**) Representative transduction current families of evoked by mechanical of hair bundle displacement from eGFP-positive cells. The displacement protocol at the bottom right applies to all three families. Scale bars are shown for each family. (**B**) Maximal transduction current recorded from eGFP-positive hair cells from the condition shown at the bottom. Symbols represent individual cells and bars represent mean ± S.D. Number of cells for each condition is shown at bottom of each bar. (**C**) Mean ± S.D current-displacement (I–X) relationships derived from P7 current families similar to those shown in panel A for eGFP-positive OHCs ($n = 6$) and eGFP-negative OHCs ($n = 20$). Data were fit with 2nd order Boltzmann equations (lines) as previously described (Stauffer and Holt, 2007). (**D-F**) Mean ± S.D. thresholds for ABRs (left) and DPOAEs (right) measured at P28–P31 from four uninjected control mice (black), four mice injected via utricle with AAV9-PHP.B-*Cmv*-eGFP (dark gray) and four mice injected via utricle with Anc80L65-*Cmv*-eGFP (light gray). Mice were injected at P1 (**D**) P7 (**E**) or P16 (**F**).

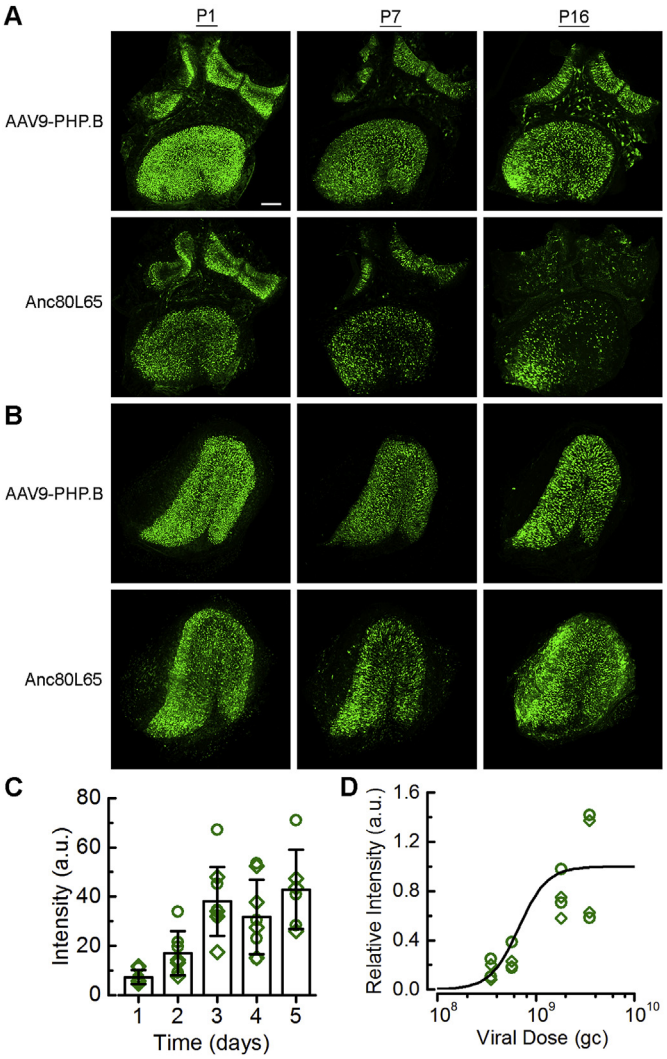

Fig. 7. Viral transduction in vestibular organs following utricle injections Representative confocal images of eGFP fluorescence in utricles, horizontal and anterior cristas (**A**) and saccules (**B**) injected via the utricle with 1 μL of AAV9-PHP.B-*Cmv*-eGFP or Anc80L65-*Cmv*-eGFP at the time points indicated above. Scale bar = 100 μm and applies to all images. (**C**) eGFP expression quantified as fluorescence intensity in arbitrary units (a.u.) as a function of days post-injection for three mice. Mean ± S.D. fluorescence intensity/area across the entire sensory epithelium was quantified for utricles (circles) and saccules (diamonds). (**D**) Relative intensity in a.u. quantified for utricles (circles) and saccules (diamonds) as a function of viral dose. The data were fit with a first order Boltzmann equation (line) that had a half maximal dose of 6.7×10^8 gc.

diluted in PBS (blocking solution) for 1 h at room temperature. Tissues were then incubated with a rabbit anti-Myosin 7a antibody (Proteus Biosciences, 1:200 dilution in blocking solution) as a hair cell marker at 37 °C overnight. A donkey anti-rabbit antibody conjugated to Alexa Fluor 633 (Life Technologies, 1:200) was used as the secondary antibody to visualize hair cells. For some experiments anti-Tuj1 was used to visualize neurons with secondary antibody conjugated to Alexa Fluor 547 (Life Technologies, 1:200). All tissues were mounted on a slide glass with VectaShield (VECTA).

4.4. Cell counts

Immunostained cochlear tissues were imaged using a Zeiss 800 confocal microscope. Laser intensity, detector gain, and image acquisition parameters were held constant. Cochlear z-stacks from

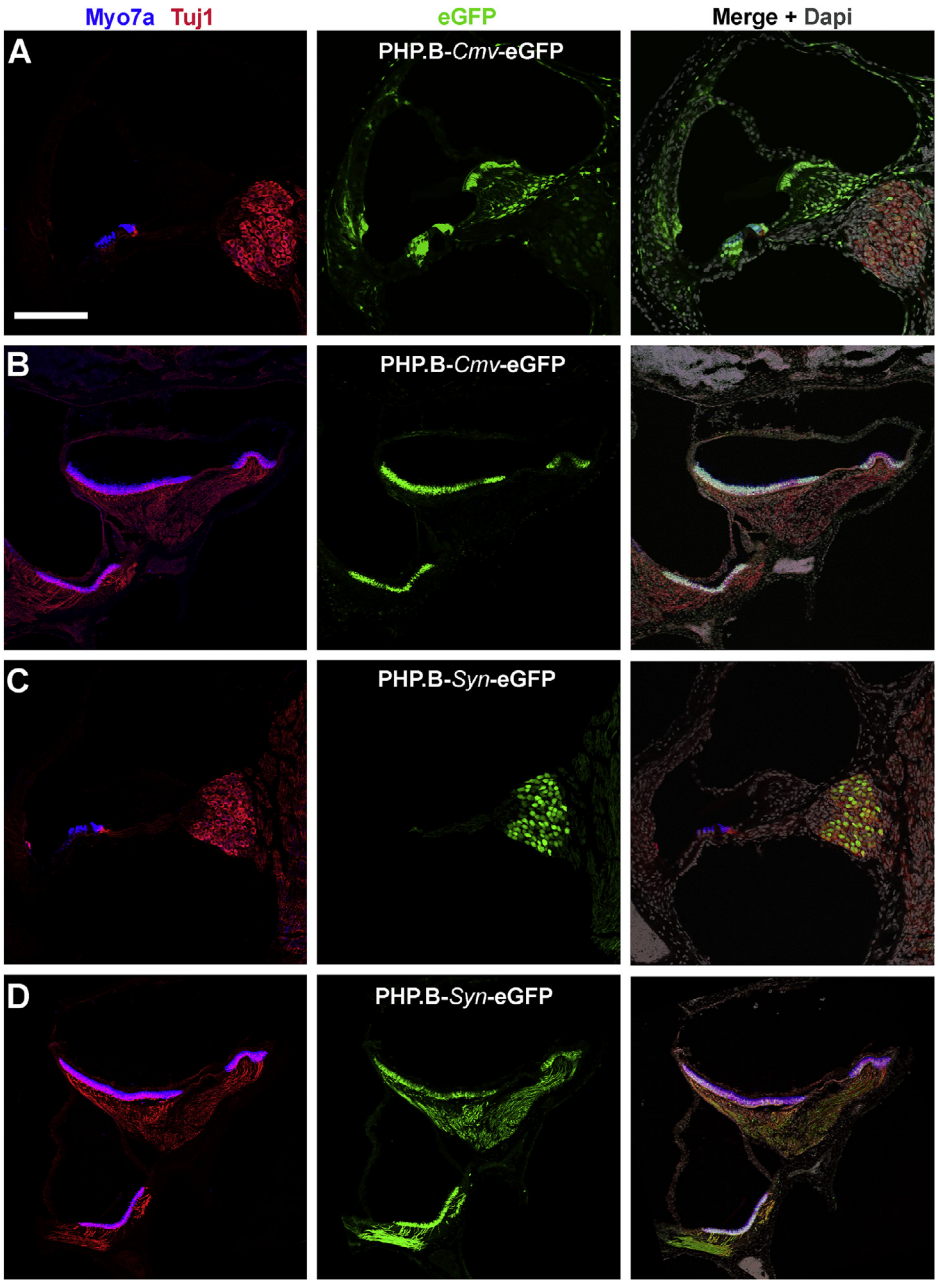

Fig. 8. Cochlear and vestibular cross-sections from utricle injected inner ears Cochlear cryosections from mice injected with 1 μL of AAV9-PHP.B-*Cmv*-eGFP at P1 via the utricle (**A**). Tissue was harvested at P15 and sections were cut, mounted and stained with anti-Myo7a, anti-Tuj1 an Dapi and imaged for all three plus eGFP. Left panel shows a merge of Myo7a and Tuj1 to illuminate hair cells and neurons, respectively. The middle panel shows eGFP fluorescence and the right panel shows the merge of all four channels. Scale bar = 200 μm and applies to all panels. (**B**) Images of vestibular organs were prepared, stained and imaged as noted above. The utricle, saccule and horizontal crista are evident. (**C**) Cochlear cryosections from mice injected with 1 μL of AAV9-PHP.B-*Syn*-eGFP at P1 via the utricle. Sections were prepared as described above. (**D**) Images of vestibular organs were prepared, stained and imaged as noted above. The utricle, saccule and horizontal crista are evident.

select regions (i.e. apex, mid, base) were obtained for each sample. The percentage of eGFP-positive IHCs and OHCs in each sample was manually and separately quantified by three blinded investigators. The number of eGFP-positive cells were divided by the total number of inner or outer hair cells, and the three separate counts were averaged for each image. Uninjected control samples were used to exclude autofluorescence. For some samples, eGFP-positive cells were quantified automatically using Imaris 3D Interactive Microscopy Visualization software to verify rigor and reproducibility of manual counts. The manual and Imaris counts were in close agreement.

4.5. Cryosections

Mouse cochlear tissue was harvested at P15 after injection on P1 via utricle with either Anc80-*Cmv*-eGFP-WPRE or AAV9-PHP.B-*Syn*-eGFP-WPRE generated at Boston Children's Hospital Viral Core. Cochlear tissue was harvested acutely after mice were euthanized with CO_2 and surrounding tissue was removed while the cochlea remained in media. Cochleae were fixed in 4% paraformaldehyde for 1 h, then decalcified in 120 mM ethylene diamine tetraacetic acid (EDTA), pH = 7.4 for 2 h. Tissues were placed in sequential baths of increasing sucrose concentration from 10%, 20%, and finally

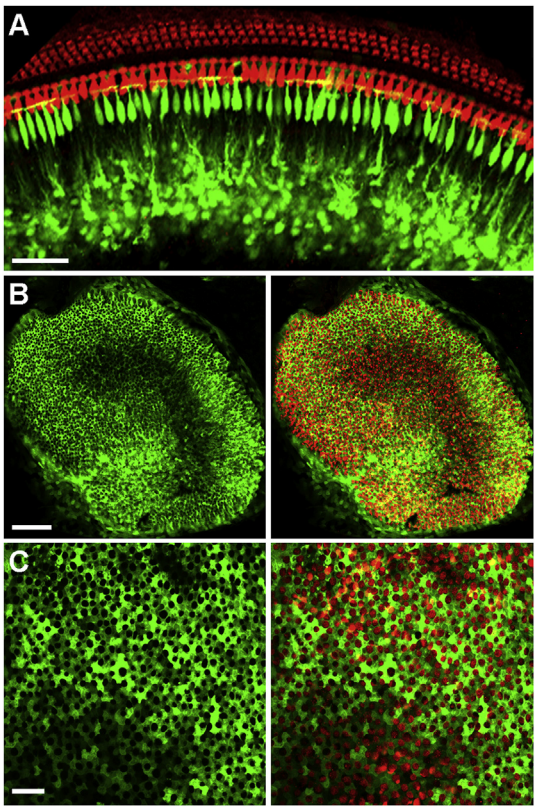

Fig. 9. GFP fluorescence with a *Gfap* promoter. Representative confocal images of inner ear tissue from P1 mice injected with 1 μL of AAV9-PHP.B-*Gfap*-eGFP via the utricle. (**A**) The tissue was harvested at P10, counterstained with anti-Myo7a and an Alexaflour547-conjugated secondary and imaged for Myo7a (red) and eGFP fluorescence (green). Scale bar = 50 μm. (**B**) Confocal Images of the mouse utricle with Myo7a (red) and eGFP fluorescence (green). Scale bar = 100 μm. (**C**) High magnification (63x) image of the same mouse utricle shown in panel B. Scale bar = 20 μm. (For interpretation of the references to color in this figure legend, the reader is referred to the Web version of this article.)

30% for 24 h to aid dehydration. Tissues were then placed in TissueTek Optimal Cutting Temperature Compound (O.C.T., Fisher) and flash frozen in methanol - dry ice mixture and subsequently held in −80° freezer until sectioning. One hour before sectioning, tissues were transferred to −20° cryostat (Leica CM1850) to equilibrate embedded tissue temperature. Tissues were sectioned at 14 μm thickness and transferred directly to Superfrost Plus glass slides (Thermo Fisher Scientific). Slides were held at 4° until staining as described in the tissue preparation and immunostaining section.

4.6. Hair cell electrophysiology

Cochlear tissues were excised and mounted on glass coverslips. Hair cells were viewed on an Examiner A1 upright microscope (Carl Zeiss) equipped with a 63x water immersion objective and differential interference contrast (DIC) optics. Electrophysiological recordings were performed at room temperature (22–24 °C) in standard perilymph solutions (in mM): 140 NaCl, 0.7 NaH2PO4, 5.8 KCl, 1.3 CaCl2, 0.9 MgCl2, 5.6 d-glucose, and 10 HEPES-NaOH, adjusted to pH 7.4 and ~310 m Osmol/kg. Vitamins (1:50) and amino acids (1:100) were added from concentrates (Invitrogen). Recording pipettes (2–4 MΩ) were pulled from R-6 glass (King Precision Glass) and filled with (in mM): 140 CsCl, 5 EGTA-CsOH, 5 HEPES, 2.5 K2ATP, 3.5 MgCl2, 0.1 CaCl2, pH 7.4 and ~285 mOsmol/kg. Whole-cell tight-seal voltage-clamp was used to record mechanotransduction currents using an Axopatch200B amplifier (Molecular Devices) with holding potential at −84 mV and pClamp 10.5 software (Molecular Devices). Data filtered at 10 kHz with a low pass Bessel filter, digitized at ≥20 kHz with a 12-bit acquisition board (Digidata 1440A). Hair bundles were deflected using a stiff glass probe mounted on a PICMA chip piezo actuator (Physik Instruments) driven by a E500 LVPZT Amplifier (Physik Instruments). The tip of thestimulus probe was fire polished to fit the hair bundle shape. Data were analyzed offline with Origin2016 software and are presented as MEAN ± SEM unless otherwise noted.

4.7. Auditory function testing

ABR and DPOAE recordings were conducted as described previously (Askew et al., 2015; Nist-Lund et al., 2019). Mice were anesthetized at time points indicated by via IP injection (0.1 ml/10 g−body weight) with 1 ml of ketamine (50 mg/ml) and 0.75 ml of xylazine (20 mg/ml) diluted into 8.25 ml of 0.9% saline. ABR and DPOAE experiments were performed at 37 °C in a sound-proof chamber. ABR and DPOAE data were collected under the same conditions, and during the same recording sessions. Prior to testing, the flap of skin and cartilage that typically obscures the entrance of the external auditory meatus was trimmed away with dissecting scissors, and sound pressure at the entrance of the ear canal was calibrated for each individual test subject at all stimulus frequencies. Acoustic stimuli were delivered directly to the studied ear through a custom probe tube speaker/microphone assembly (EPL PXI Systems) consisting of two electrostatic earphones (CUI Miniature Dynamics) to generate primary tones and a Knowles miniature microphone (Electret Condenser) to record ear-canal sound pressure. To test hearing function, mice were presented pure tone stimuli of 5.6 kHz, 8 kHz, 11.3k Hz, 16 kHz, 22.6 kHz, or 32 kHz. To determine ABR thresholds, sound pressure levels were used between 10 and 110 dB in 5 dB steps. Using an alternating polarity stimulus, 512 responses were collected and averaged for each sound pressure level. Waveforms with amplitude larger than 15 μV (peak-to-trough) were discarded by an “artifact reject” function. Sound stimuli consisted of 5-ms tone bursts (0.5 ms rise−fall with a $\cos^2$ onset, delivered at 40 Hz). ABR signals were collected using subcutaneous needle electrodes inserted at the pinna (active electrode), vertex (reference electrode), and rump (ground electrode). ABR potentials were amplified (10,000x), pass-filtered (0.3–10 kHz), and digitized using custom data acquisition software (LabVIEW). Sound stimuli and electrode voltage were sampled at 40-μs intervals using a digital I–O board (National Instruments) and stored for offline analysis. Threshold was defined visually as the lowest decibel level at which peak I could be detected and reproduced with increasing sound intensities. ABR thresholds were averaged within each experimental group and used for statistical analysis. For DPOAE recordings, the same frequencies used for ABR were used in conjunction with primary tones at a frequency ratio of 1.2 (f2/f1) for the generation of DPOAEs at 2f1-f2, where the f2 level was 10 dB sound pressure level below f1 level for each f2/f1 pair. The f2 levels were swept in 10-dB steps from 10 to 80 dB. Waveform and spectral averaging were used at each level to increase the signal-to-noise ratio of the recorded ear-canal sound pressure. The amplitude of the DPOAE at 2f1-f2 was extracted from the averaged spectra, along with the noise floor at nearby points in the spectrum. Iso-response curves were interpolated from plots of DPOAE amplitude versus sound level. Threshold was defined as the f2 level required to produce DPOAEs above 0 dB.

4.8. Balance assessment

Balance assessments were carried out by the Neurobehavioral Core at Boston Children’s Hospital (IDDRC). Vestibular function was

assessed using the rotarod balance test. The rotarod performance involved placement of mice on a rod in an enclosed housing that began rotating at 4 r.p.m. and accelerated at a rate of 0.1 r.p.m. s^{-1}. On the initial training day, the mice were placed on the rods for 5 min to gain familiarity with the equipment. The next day, the animals were placed on the rods for a total of 5 trials. A 5-min resting period was imposed between trials. The length of time the animals were able to remain on the device before dropping onto the instrumented floor of the housing was displayed on a timer and recorded after each test run.

CRediT authorship contribution statement

John Lee: Methodology, Investigation, Formal analysis, Visualization, Writing - original draft. **Carl Nist-Lund:** Methodology, Investigation, Formal analysis, Visualization, Writing - original draft. **Paola Solanes:** Conceptualization, Resources, Writing - original draft. **Hannah Goldberg:** Investigation, Formal analysis, Writing - original draft. **Jason Wu:** Investigation, Formal analysis, Writing - original draft. **Bifeng Pan:** Investigation, Formal analysis, Writing - original draft. **Bernard L. Schneider:** Conceptualization, Resources, Writing - original draft. **Jeffrey R. Holt:** Conceptualization, Resources, Methodology, Formal analysis, Visualization, Writing - original draft, Supervision, Funding acquisition.

Acknowledgements

The authors would like to thank Yukako Asai for initiating the project and Gwenaelle Geleoc for many helpful discussions. This work was supported by the IDDRC (grant # 1U54HD090255) and the Neurodevelopmental Behavioral and Viral Cores at Boston Children's Hospital. Gene therapy research in the Holt/Geleoc lab is supported by the Jeffrey and Kimberly Barber Fund for Gene Therapy Research, The Usher Syndrome Society and Foundation Pour L'Audition.

References

Akil, O., Seal, R.P., Burke, K., Wang, C., Alemi, A., During, M., Edwards, R.H., Lustig, L.R., 2012 Jul 26. Restoration of hearing in the VGLUT3 knockout mouse using virally mediated gene therapy. Neuron 75 (2), 283–293.

Askew, C., Rochat, C., Pan, B., Asai, Y., Ahmed, H., Child, E., Schneider, B.L., Aebischer, P., Holt, J.R., 2015 Jul 8. Tmc gene therapy restores auditory function in deaf mice. Sci. Transl. Med. 7 (295), 295ra108.

Chien, W.W., Isgrig, K., Roy, S., Belyantseva, I.A., Drummond, M.C., May, L.A., Fitzgerald, T.S., Friedman, T.B., Cunningham, L.L., 2016 Feb. Gene therapy restores hair cell stereocilia morphology in inner ears of deaf whirler mice. Mol. Ther. 24 (1), 17–25.

Dalkara, D., Byrne, L.C., Klimczak, R.R., Visel, M., Yin, L., Merigan, W.H., Flannery, J.G., Schaffer, D.V., 2013 Jun 12. In vivo-directed evolution of a new adeno-associated virus for therapeutic outer retinal gene delivery from the vitreous. Sci. Transl. Med. 5 (189), 189ra76.

Deverman, B.E., Pravdo, P.L., Simpson, B.P., Kumar, S.R., Chan, K.Y., Banerjee, A., Wu, W.L., Yang, B., Huber, N., Pasca, S.P., Gradinaru, V., 2016 Feb. Cre-dependent selection yields AAV variants for widespread gene transfer to the adult brain. Nat. Biotechnol. 34 (2), 204–209.

Dulon, D., Papal, S., Patni, P., Cortese, M., Vincent, P.F., Tertrais, M., Emptoz, A., Tlili, A., Bouleau, Y., Michel, V., Delmaghani, S., Aghaie, A., Pepermans, E., Alegria-Prevot, O., Akil, O., Lustig, L., Avan, P., Safieddine, S., Petit, C., El-Amraoui, A., 2018 Aug 1. Clarin-1 gene transfer rescues auditory synaptopathy in model of Usher syndrome. J. Clin. Investig. 128 (8), 3382–3401.

Emptoz, A., Michel, V., Lelli, A., Akil, O., Boutet de Monvel, J., Lahlou, G., Meyer, A., Dupont, T., Nouaille, S., Ey, E., Franca de Barros, F., Beraneck, M., Dulon, D., Hardelin, J.P., Lustig, L., Avan, P., Petit, C., Safieddine, S., 2017. Local gene therapy durably restores vestibular function in a mouse model of Usher syndrome type 1G. Proc Natl Acad Sci U S A. 114 (36), 9695–9700. https://doi.org/10.1073/pnas.1708894114.

Gu, X., Chai, R., Guo, L., Dong, B., Li, W., Shu, Y., Huang, X., Li, H., 2019 Jan 24. Transduction of adeno-associated virus vectors targeting hair cells and supporting cells in the neonatal mouse cochlea. Front. Cell. Neurosci. 13, 8.

György, B., Sage, C., Indzhykulian, A.A., Scheffer, D.I., Brisson, A.R., Tan, S., Wu, X., Volak, A., Mu, D., Tamvakologos, P.I., Li, Y., Fitzpatrick, Z., Ericsson, M., Breakefield, X.O., Corey, D.P., Maguire, C.A., 2017 Feb 1. Rescue of hearing by gene delivery to inner-ear hair cells using exosome-associated AAV. Mol. Ther. 25 (2), 379–391.

György, B., Meijer, E.J., Ivanchenko, M.V., Tenneson, K., Emond, F., Hanlon, K.S., Indzhykulian, A.A., Volak, A., Karavitaki, K.D., Tamvakologos, P.I., Vezina, M., Berezovskii, V.K., Born, R.T., O'Brien, M., Lafond, J.F., Arsenijevic, Y., Kenna, M.A., Maguire, C.A., Corey, D.P., 2019 Nov 20. Gene transfer with AAV9-PHP.B rescues hearing in a mouse model of usher syndrome 3A and transduces hair cells in a non-human primate. Mol. Ther. Methods Clin. Dev. 13, 1–13.

Hernandez, V.H., Gehrt, A., Reuter, K., Jing, Z., Jeschke, M., Mendoza Schulz, A., Moser, T., 2014. Optogenetic stimulation of the auditory pathway. JCI 124, 1114–1129.

Isgrig, K., McDougald, D.S., Zhu, J., Wang, H.J., Bennett, J., Chien, W.W., 2019 Jan 25. AAV2.7m8 is a powerful viral vector for inner ear gene therapy. Nat. Commun. 10 (1), 427.

Jones, S.M., Subramanian, G., Avniel, W., Guo, Y., Burkard, R.F., Jones, T.A., 2002. Stimulus and recording variables and their effects on mammalian vestibular evoked potentials. J. Neurosci. Methods 118 (1), 23–31.

Keppeler, D., Merino, R.M., Lopez de la Morena, D., Bali, B., Huet, A.T., Gehrt, A., Moser, T., 2018. Ultrafast optogenetic stimulation of the auditory pathway by targeting-optimized chronos. EMBO 37 (24), e99649.

Kilpatrick, L.A., Li, Q., Yang, J., Goddard, J.C., Fekete, D.M., Lang, H., 2011 Jun. Adeno-associated virus-mediated gene delivery into the scala media of the normal and deafened adult mouse ear. Gene Ther. 18 (6), 569–578.

Kim, M.A., Ryu, N., Kim, H.M., Kim, Y.R., Lee, B., Kwon, T.J., Bok, J., Kim, U.K., 2019 Jan 11. Targeted gene delivery into the mammalian inner ear using synthetic serotypes of adeno-associated virus vectors. Mol. Ther. Methods Clin. Dev. 13, 197–204.

Landegger, L.D., Pan, B., Askew, C., Wassmer, S.J., Gluck, S.D., Galvin, A., Taylor, R., Forge, A., Stankovic, K.M., Holt, J.R., Vandenberghe, L.H., 2017 Mar. A synthetic AAV vector enables safe and efficient gene transfer to the mammalian inner ear. Nat. Biotechnol. 35 (3), 280–284.

Nist-Lund, C.A., Pan, B., Patterson, A., Asai, Y., Chen, T., Zhou, W., Zhu, H., Romero, S., Resnik, J., Polley, D.B., Géléoc, G.S., Holt, J.R., 2019 Jan 22. Improved TMC1 gene therapy restores hearing and balance in mice with genetic inner ear disorders. Nat. Commun. 10 (1), 236.

Pan, B., Askew, C., Galvin, A., Heman-Ackah, S., Asai, Y., Indzhykulian, A.A., Jodelka, F.M., Hastings, M.L., Lentz, J.J., Vandenberghe, L.H., Holt, J.R., Géléoc, G.S., 2017 Mar. Gene therapy restores auditory and vestibular function in a mouse model of Usher syndrome type 1c. Nat. Biotechnol. 35 (3), 264–272.

Stauffer, E.A., Holt, J.R., 2007 Dec. Sensory transduction and adaptation in inner and outer hair cells of the mouse auditory system. J. Neurophysiol. 98 (6), 3360–3369.

Suzuki, J., Hashimoto, K., Xiao, R., Vandenberghe, L.H., Liberman, M.C., 2017 Apr 3. Cochlear gene therapy with ancestral AAV in adult mice: complete transduction of inner hair cells without cochlear dysfunction. Sci. Rep. 7, 45524.

Tao, Y., Huang, M., Shu, Y., Ruprecht, A., Wang, H., Tang, Y., Vandenberghe, L.H., Wang, Q., Gao, G., Kong, W.J., Chen, Z.Y., 2018 Apr. Delivery of adeno-associated virus vectors in adult mammalian inner-ear cell subtypes without auditory dysfunction. Hum. Gene Ther. 29 (4), 492–506.

Zinn, E., Pacouret, S., Khaychuk, V., Turunen, H.T., Carvalho, L.S., Andres-Mateos, E., Shah, S., Shelke, R., Maurer, A.C., Plovie, E., Xiao, R., Vandenberghe, L.H., 2015 Aug 11. In silico reconstruction of the viral evolutionary lineage yields a potent gene therapy vector. Cell Rep. 12 (6), 1056–1068.